Supporting Information:
The three-dimensional structure of fine-scale, vertical velocities in the Southern Ocean inferred from space

May 13, 2026

Andrew F. Thompson[1*], Lilian A. Dove[2,3], Yann-Treden Tranchant[4,5], Benoit Legresy[4,6], Beatriz Peña Molino[4,6], Laura Herraiz Borreguero[4,6], Zichang He[1], Patrice Klein[1,7]

[1]Environmental Science and Engineering, California Institute of Technology, Pasadena, CA, USA
[2]Department of Earth, Environmental & Planetary Sciences, Brown University, Providence, RI, USA
[3] School of Earth and Atmospheric Sciences, Georgia Institute of Technology, Atlanta, GA, USA
[4]Australian Antarctic Program Partnership, Hobart, TAS, Australia
[5] Institute for Marine and Antarctic Studies, University of Tasmania, Hobart, TAS, Australia
[6]Commonwealth Scientific Industrial Research Organisation, Hobart, TAS, Australia
[7]LMD/IPSL, CNRS, Ecole Normale Supérieure, Polytechnique, PSL Research University, 75005 Paris, France

Corresponding author: *andrewt@caltech.edu*

Table of Contents

1. Supplementary Figure 1
2. Supplementary Figure 2
3. Supplementary Figure 3
4. Supplementary Figure 4
5. Supplementary Figure 5
6. Supplementary Figure 6
7. Supplementary Figure 7
8. Supplementary Figure 8

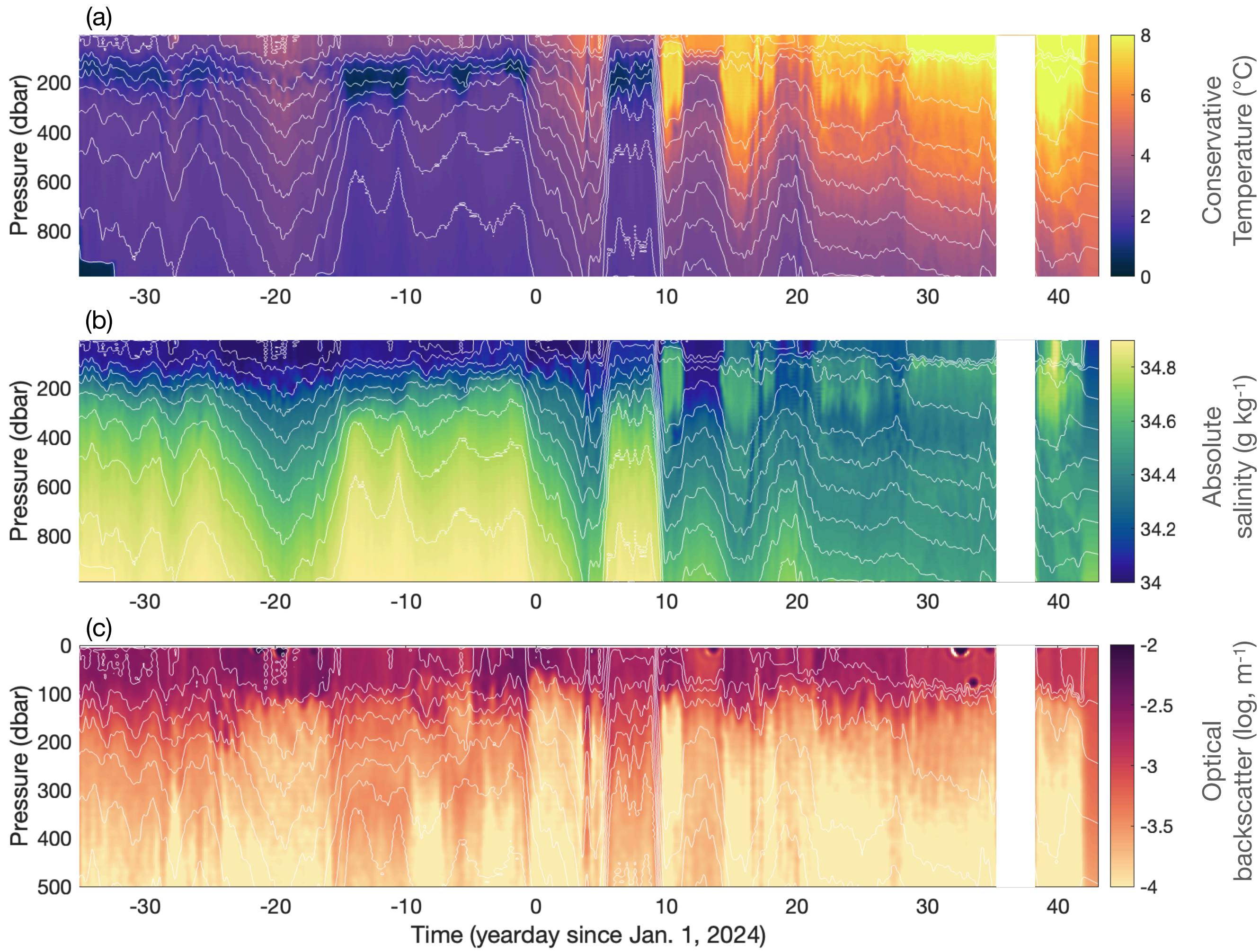

Supplementary Figure 1: **FOCUS glider observations.** Depth-time series (a) conservative temperature (°C), (b) absolute salinity (g kg^{-1}), and (c) optical backscatter (m^{-1} along the trajectory of glider SG659 (Figure 1). The white lines show potential density surfaces, σ_0 with a contour interval of 0.1 kg m^{-3}. The tracer properties show the same structuring by mesoscale features as SG681 (Figure 2b), and show finer scale variability in backscatter around the edges of mesoscale eddies. Note that the depth scale in panel (c) is different because the optical sensor only sampled to 500 m.

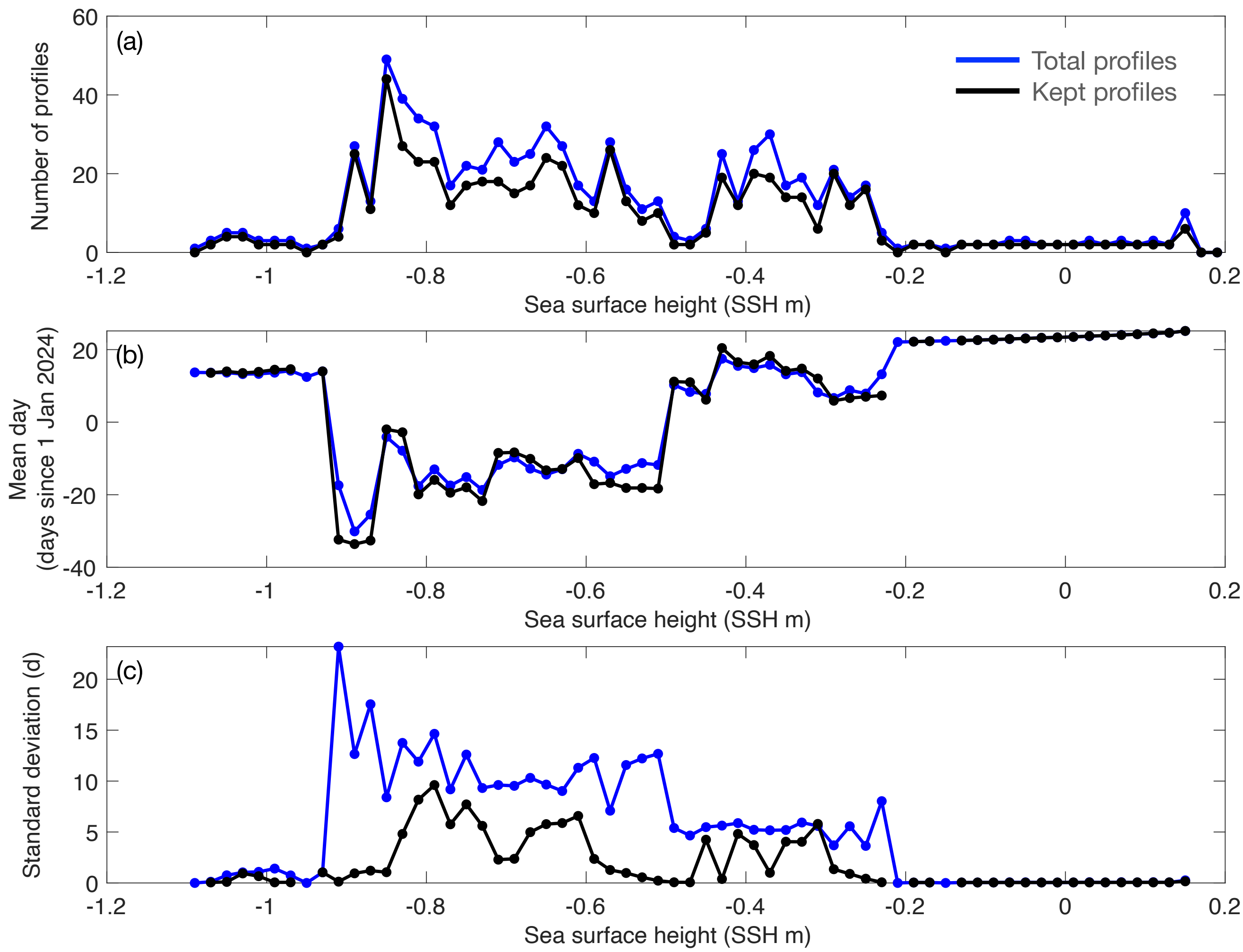

Supplementary Figure 2: **Statistics related to the SSH-density relationship.** (a) Number of glider profiles within the SSH bins (2 cm spacing) in total (blue) and after removing those collected one standard deviation away from the mean date of the profiles. (b) Mean time (days since 1 January, 2024) when the profiles were collected in each SSH bin. (c) Standard deviation of the time when profiles were collected for each SSH bin.

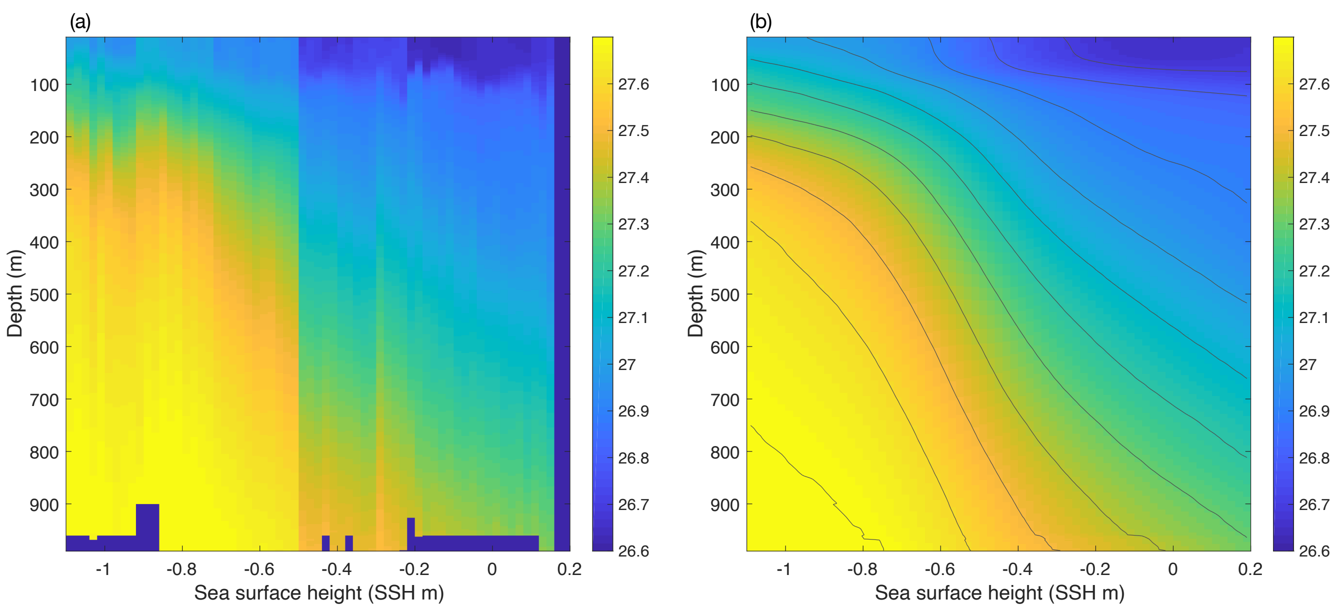

Supplementary Figure 3: **SSH-Density relationship.** (a) Distribution of potential density as a function of depth and ADT prior to smoothing. The abrupt transition around ADT = -0.5 m is aligned with the Polar Front (PF) where there are few glider measurements due to the strong gradient in SSH at the core of the PF. (b) Smoothed distribution of potential density as a function of depth and sea surface height (as in Figure 2b). Details of the smoothing approach is provided in the Methods.

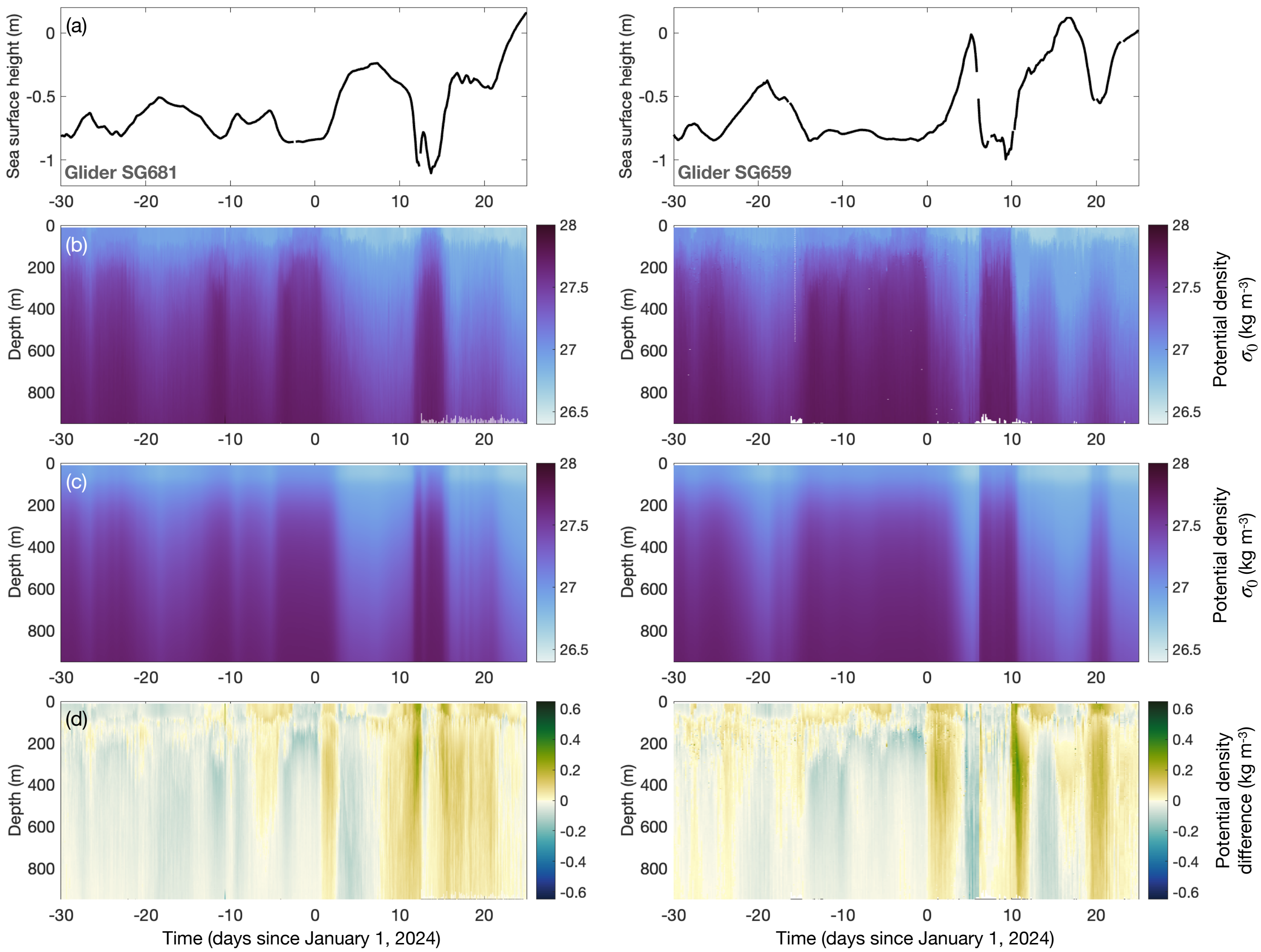

Supplementary Figure 4: **Density reconstruction for two ocean gliders, SG681 (left panels) and SG659 (right panels).** (a) Sea surface height (m) interpolated to the position of each glider using the DUACS ADT daily product. (b) Measured potential density (σ_0, kg m^{-3}) as a function of depth and along the glider trajectory. (c) Reconstructed potential density (kg m^{-3}) as a function of depth and position along the glider trajectory using the SSH values in panel (a) and the SSH-σ_0 relationship in Figure 2b (kg m^{-3}). (d) Difference between measured and reconstructed potential density (difference between panels (b) and (c)).

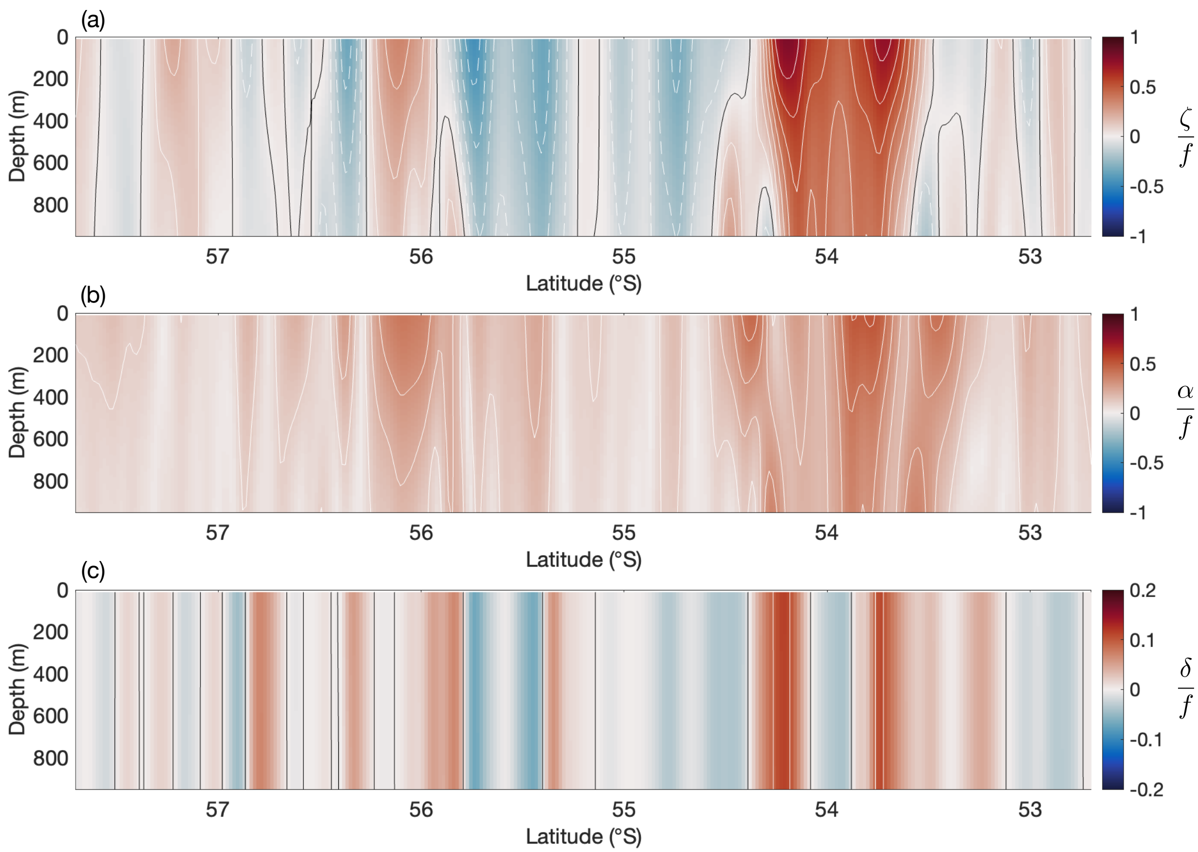

Supplementary Figure 5: **Vorticity, strain, divergence.** Distributions of normalized (a) vorticity (ζ/f), (b) strain (α/f), and (c) divergence (δ/f) for the along-swath section shown in Figure 4e-h. There are no vertical variations in the divergence field because the velocities are determined from the thermal wind relationship.

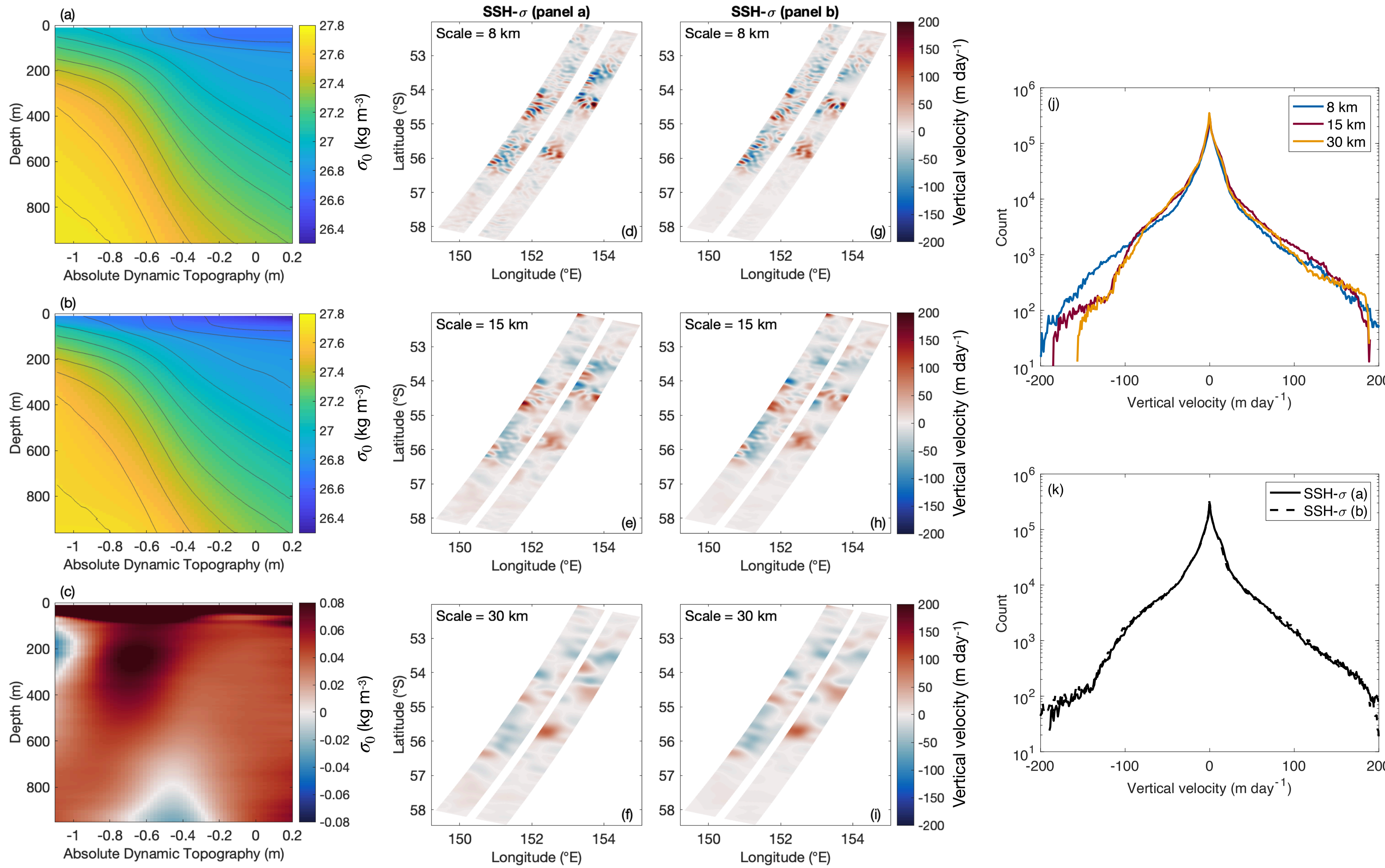

Supplementary Figure 6: **Vertical velocity sensitivity figure.** (a) SSH-σ relationship as described in §**2.2**. (b) SSH-σ relationship using a reduced vertical smoothing of 5-m half width at half maximum. (c) Difference between panel (a) and (b); most of the variations occur in the mixed layer. (d-i) Sensitivity of the vertical velocity inversion to the SSH-σ relationship (columns) and the horizontal smoothing of the **Q** field. In each panel, the horizontal distribution of w at 200 m is shown on January 28, 2024 (Figure 4) The smoothing uses a Gaussian filter where the kernel has a (d,g) 8-km full width at half maximum, (e,h) 15-km full width at half maximum, and (f,i) 30-km full width at half maximum. (j) Histogram of w for all depths from panels (d; blue curve), (e; red curve), and (f; yellow curve). (k) Histogram of w for all depths from panels (e; solid curve), (h; dashed curve).

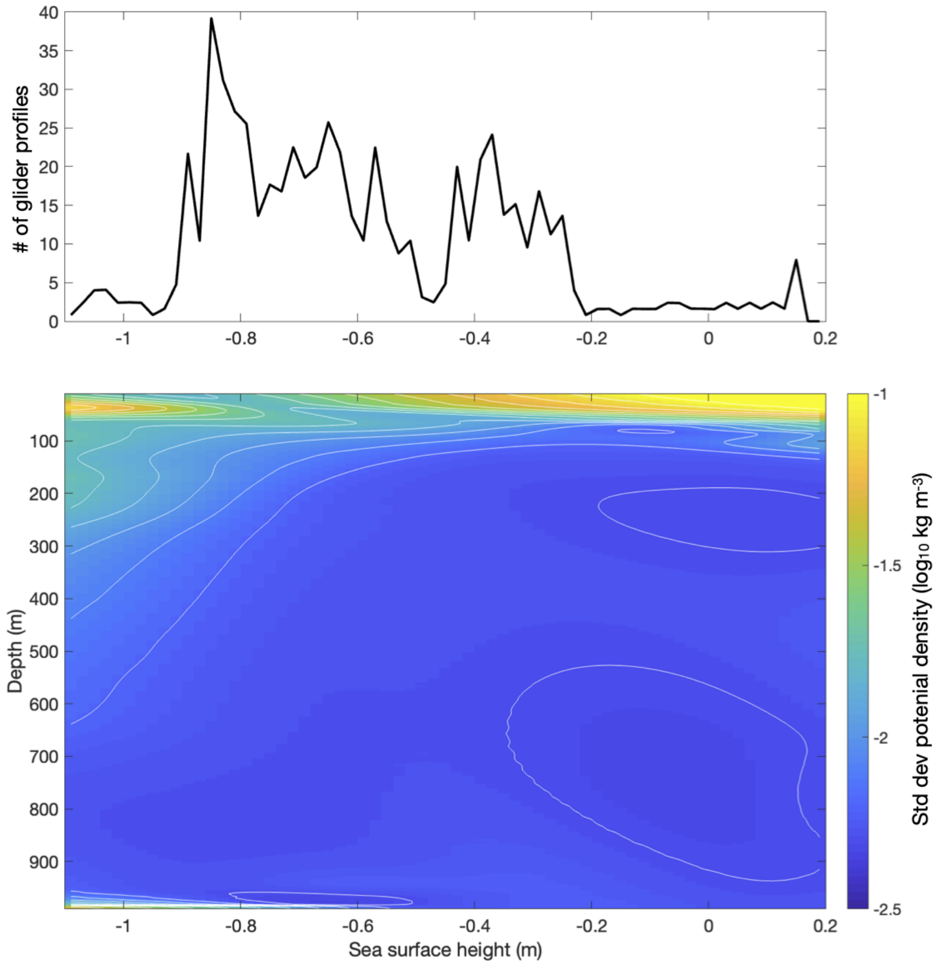

Supplementary Figure 7: **Monte Carlo assessment of sensitivity to data availability. Upper panel**) Average number of profiles used for each SSH bin (0.02 m) to create 500 realizations of the SSH-σ relationship. This represents a 20% reduction in glider profiles from the full data set. The removed glider profiles are chosen at random from the full data set. (**Lower panel**) Standard deviation of the potential density from the 500 realizations; the colorscale is logarithmic such that $10^{-2} = 0.01$ kg m^{-3}.

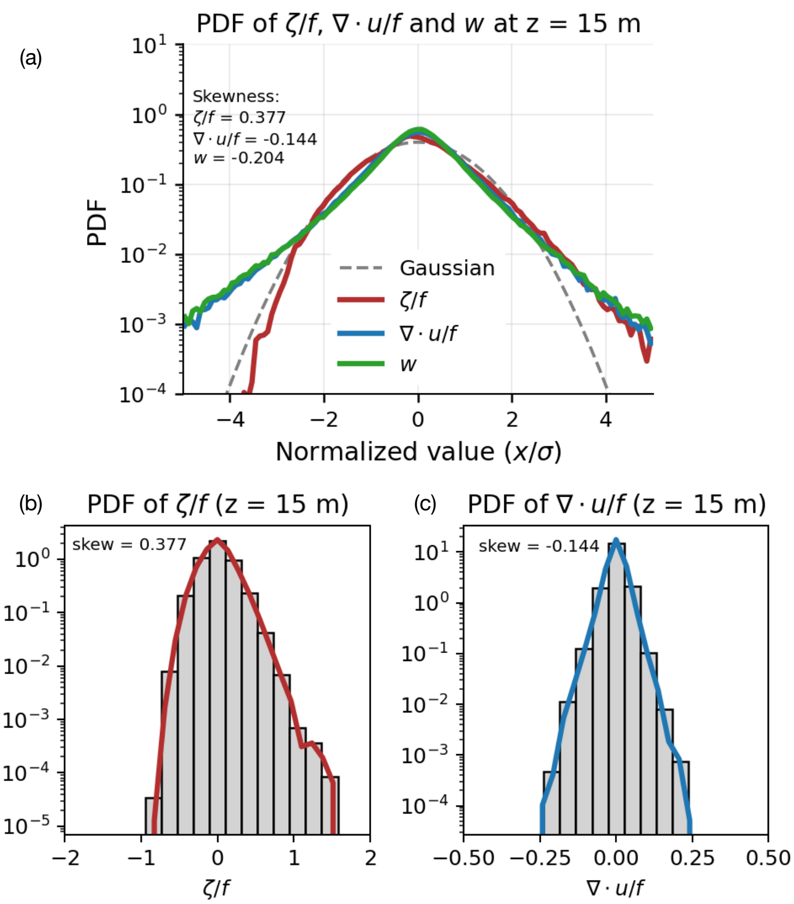

Supplementary Figure 8: **Statistics of the COMPAS numerical model output.** (a) PDF of normalized vorticity (red curve), horizontal divergence (blue curve), and vertical velocity (green curve) from the 3-km COMPAS model output. The vorticity and divergence curves are expanded in panels (b) and (c), respectively, to highlight the different skewness characteristics.